24

Lymphoblastoid Cells Exposed to Low-Frequency Magnetic Fields

Study by Atomic Force Microscopy

Settimio Grimaldi, Marco Girasole, and Antonio Cricenti

1. Introduction

Since the appearance of the first pioneering article in the 1970s, particular efforts have been made to study the effect of exposure to electric and magnetic fields (EMFs) on living matter ***(1–10)***. The initial interest in radio frequency and microwaves has shifted to include the nonthermal, and essentially magnetic, effect of extremely low frequencies (ELF, 1–300 Hz), in particular the 50 and 60 Hz of the electric power system ***(3,4,9)***. The density of normal ELF fields is usually below 0.1 μT, but values of 0.5 μT may be found in front of television sets and computer monitors ***(11)*** as well as at a distance of 50 m from 300-kV high-voltage power lines ***(12)***. Values up to two to three orders of magnitude higher can be found near some domestic appliances or in some industrial processes, and pulsed magnetic fields in the range 1–10 mT are used in nuclear magnetic resonance imaging and for the therapy of soft tissue or nonhealing bone fractures ***(1)***.The increasing interest in ELF fields has been partially motivated by epidemiological reports of an increase in some types of cancer and leukemia in children ***(13,14)*** and workers exposed to high levels of ambient fields. Carcinogenesis is considered to be a multistep process consisting of initiation–promotion–progression stages ***(15)***. Although ELF magnetic fields are not considered sufficiently energetic to interact with DNA and initiate a cancerous process, they could, by acting on cellular receptors, affect cell proliferation and modulate the promotion or progression stage. Although exposure to a high-intensity, 50–60 Hz, magnetic field (MF) has been demonstrated to be effective in modifying the growth rate of cells ***(16)***, and a distur-

From: *Methods in Molecular Biology, vol. 242: Atomic Force Microscopy: Biomedical Methods and Applications*
Edited by: P. C. Braga and D. Ricci © Humana Press Inc., Totowa, NJ

bance of melatonin rhythm has also been found-supporting the hypothesis of melatonin-mediated breast cancer development ***(17)***-no final evidence of a link between tumor and field MF exposure has been reported. In light of this, however, particular attention must be paid to studies performed on cells of the immune system because of its fundamental barrier action against pathogens and cancer development.

One of the main difficulties in the study of electric and magnetic field interaction with cells and in the extension of the results to different biosystems arises from the strong dependence of the response pathway on such field parameters as intensity, exposure time, wave shape, and especially the nonlinear frequency dependence. Because the plasma membrane can be regarded as a (nonideal) capacitor with a fixed frequency curve ***(4)***, differences in the induced effects between low frequency fields, which can modify the membrane potential, and high frequency fields, which can easily penetrate cells, are expected. Less understandable is how and why specific frequency windows (sometimes as narrow as few Hz) seem to be particularly effective in producing biophysical or biochemical cell modifications. Little is known as well about the mechanism of action when the field intensity is close to the thermal noise limit. Another complication is the known fact that present inhibitory or stimulatory behavior depends on the cell line used.

Even though no theory has completely succeeded in describing the interaction between field and cells, different models have been proposed to explain the experimental results ***(2,9,18–20)***. These models converge in attributing a crucial role to Ca^{2+} ions, suggesting a change in transport and/or in reactivity of Ca^{2+} induced by particular frequencies of the applied field. Such changes can induce a nonphysiological concentration of these ions within the cell ***(21,22)*** that can trigger biochemical and genetic modifications ***(23)***. It is also accepted that the plasma membrane is one of the target sites of the field, so characterizing its modifications is important to understanding the nature of the interaction. A high-resolution surface-characterizing technique such as atomic force microscopy (AFM) can be a helpful tool in such a study. Recent reviews of this technique and some of its successes that justify its increasing prestige in the study of biological samples can be found in literature ***(24–29)***.

A large number of experimental studies have been done both in vivo and in vitro on this subject. With regard to in vivo experiments concerning immune system cells, it has been demonstrated that nonthermal ELF MF exposure can modify the number of leukocytes, the response to inflammations ***(30,31)***, as well as the activity of natural killer cells in blood ***(32)***. In vitro studies of ELF MF in the range of 1–10 mT have shown membrane surface modifications as evidenced by microscopy, as well as a decrease in conductivity induced by 2.5-mT, 50-Hz exposure in K562 cells ***(5,33)***. In addition, effects on calcium fluxes, DNA synthesis, and RNA transcription have been reported, such as an increase

in cytosolic Ca^{2+} concentration in HL-60 cells exposed to a 0.1-mT MF ***(21)***, the same effect on T lymphoblast cells ***(34)***, changes in protein kinase activity in Raji cells exposed to 2-mT, 50-Hz MF ***(10)***, an increase of uridine (RNA) uptake in HL-60 cells exposed to 1-mT, 60-Hz MF ***(35)***, and reduction in thymidine (DNA) uptake in human peripheral blood lymphocytes ***(36)*** exposed to 6-mT, 3-Hz (square wave) MF. It must be noted that some of the reported effects on DNA or RNA are in some way calcium-dependent or calcium-mediated so that a crucial role for calcium as target of ELF fields clearly emerges.

2. Materials

2.1. Exposure Solenoid

The MF was generated by a sinusoidal current flowing in a solenoid (height 40 cm, diameter 20 cm) made of 600 turns of 0.2-cm (diameter) copper wires wound around an asbestos tube and placed with its axis vertical, so that the magnetic flux was perpendicular to the sample ***(10)***. The sample holder consisted of a water jacket (temperature regulated) container suspended at the centre of the solenoid. The current was driven by a 50-Hz power supply through a variable autotransformer generating a flux of 2 mT (root mean square [rms]) for an applied voltage of 12 V (rms). With these parameters, the surface temperature of the solenoid during the experiment is always below 30°C; no warming of the sample is possible. In order to maintain a fixed temperature during the exposure and to avoid morphological modifications induced by temperature variations ***(37)***, the sample was carefully maintained at a constant temperature of 37 ± 0.3°C by the temperature control system. The field intensity (measured with a calibrated Hall probe) varied within 5% of its central value inside the cylindrical exposure space.

The presence of a homogeneous electric field component parallel to the applied MF is very much debated in experiments with electromagnetic radiation because some researchers report effects induced by weak electric fields (although this still in discussion) ***(38)***.

Surely one way to bypass such a problem is to use EMFs in which one of the components is clearly predominant with respect to the other. This is achieved in experiments with ELF fields in which the magnetic component is in the mT range. For instance, in our experiments we estimated that the residual electric component ***(10)*** on the sample was below 80 μV/cm, which is very close to the minimum theoretical electric field to which a cell may respond ***(38)***, and its putative contribution can be considered negligible compared to the magnetic component.

2.2. Sample Preparation

1. Lymphocyte B cells transformed by Epstein-Barr virus.
2. RPMI (Gibco Laboratories).

3. Trypan blue dye.
4. Poly-lysine-treated glass.

The cell line used was lymphocyte B cells transformed by the Epstein–Barr virus ***(39)***, also known as Raji cells (from ATCC; Rockville, MD), grown at 37°C in RPMI (from Gibco Laboratories; Paisley, Scotland UK) supplemented with 10% fetal calf serum (Gibco), penicillin (110 U/mL), streptomycin (100 µg/mL), and perfused with 5% CO_2 as carbon source (which was provided also during the MF exposure). At confluence, the cells were divided into two samples and placed in 25-mL Corning flasks filled with the above mentioned medium. One sample was exposed to the sinusoidal MF continuously for 9, 15, 24, 44, and 64 h; the sham sample (control) was placed under the same conditions in a solenoid with no field. After the exposure, cell viability was determined by Trypan blue dye exclusion. This invariably showed a negligible amount of dead cells. Exposed and non-exposed cells were attached to poly-lysine treated glass cover slides, fixed in paraformaldehyde (2% for 10 min), washed with a physiological solution, washed again with distilled water to avoid salt deposition, air dried, and finally observed in air by AFM.

This way of preparing dried samples is often used in air performed microscopy experiments to reduce as much as possible any artifact on cell morphology or viability. It allows good and reproducible results ***(40,41)*** because the samples are not damaged or weakly stressed, and they remain stable for long periods of time. Moreover, to distinguish between real effects and artifacts, a control sample was prepared for each exposed sample.

2.3. AFM Instrument and Data Analysis

Our homemade AFM instrument was described in detail elsewhere ***(42)***; briefly, it consists of a stainless-steel unit made of two separable cylindrical supports equipped with a vibration isolating system. The lower unit contains the sample holder mounted at the top of a piezo electric scanner that allows a maximal scan size of $40 \times 40 \times 6$ µm. Additionally an *x-y-z* motor-controlled translator is used to select suitable areas of the sample. The upper unit contains the cantilever holder, the mirror deflection system, and a four-sector position-sensitive photodiode used as deflection detector. An electronic feedback loop is used to integrate the optical signal and maintain a constant cantilever deflection during the data acquisition. Our instrument has been previously successfully used for imaging biological samples ***(29,43,44)***; the typical lateral resolution is about 10 nm and around 0.1 nm in the *z* direction (for a sample placed on a flat surface; **ref. *29***). In the present work, several reported images have a relatively low lateral resolution because of the large range required to observe a whole cell and because of the characteristics of our acquisition soft-

ware, which allows a maximum of 256 points per row (regardless of the range of the image). However, a number of smaller images were acquired (data not shown) in which features as small as 20 nm or less were distinguishable.

The AFM measurements were performed in air (at room temperature), with the microscope working in the weak repulsive regime of contact mode with a force of less than 1 nN from zero cantilever deflection. Gold-coated Si_3N_4 (Park Scientific Instruments; Sunnyvale, CA) microlevers with a spring constant of 0.023 N/m and an expected statistical apical radius of 5–30 nm were used. Constant force and lateral friction images were acquired simultaneously with a typical scan rate of 3–4 s/row (256 points/row). The lateral friction-imaging mode has been found very powerful in this work because of its sensitivity to small structures, such as microvilli, that protrude from a large and corrugated surface.

The raw data were treated only using background subtraction and the reproducibility of data (including the absence of sample damage attributable to the measurement procedure) was successfully tested by imaging the same cells on different days. In relation to the still open question of the elastic deformation of soft biological samples because of the contact mode measurement method, it should be noted that the probe force (which was the same in all the samples analyzed) is very small and in the range commonly reported in the literature for similar contact mode experiments. Anyway, a rough estimation ***(24)*** of the elastic compression of a protein characterized by a Young's modulus of about 20 kg_f/cm^2 (i.e., well below the value expected in the case of a whole cell) carried out a value of elastic deformation that is largely inside the experimental error reported by us. The fit of data was calculated using the Kaleidagraph for Windows (Synergy Software version 3.08) software package.

3. Methods

3.1. Image Collection and Interpretation

In **Figs. 1** and **2**, AFM topological and lateral friction images, respectively, of typical cells unexposed (**Figs. 1A** and **2A**) and exposed continuously for 9, 24, and 64 h to MF (**Figs. 1B–D** and **2B–D**, respectively) are shown. Unexposed cells (**Figs. 1A** and **2A**) show a characteristic domed shape and have height values (defined as top cell height minus cell background) ranging between 2.1 and 2.5 μm. The cells appear highly structured and covered by microvilli, which are recognized both in the topographic (**Fig. 1A**) and lateral friction (**Fig. 2A**) images. Microvilli are protrusions, mainly composed of actin polymers, of the lymphocyte membrane known to be very sensitive to environmental variations ***(36,45,10)*** and important in the recognition of inflammations sites. In the untreated sample it is also possible to see, on the

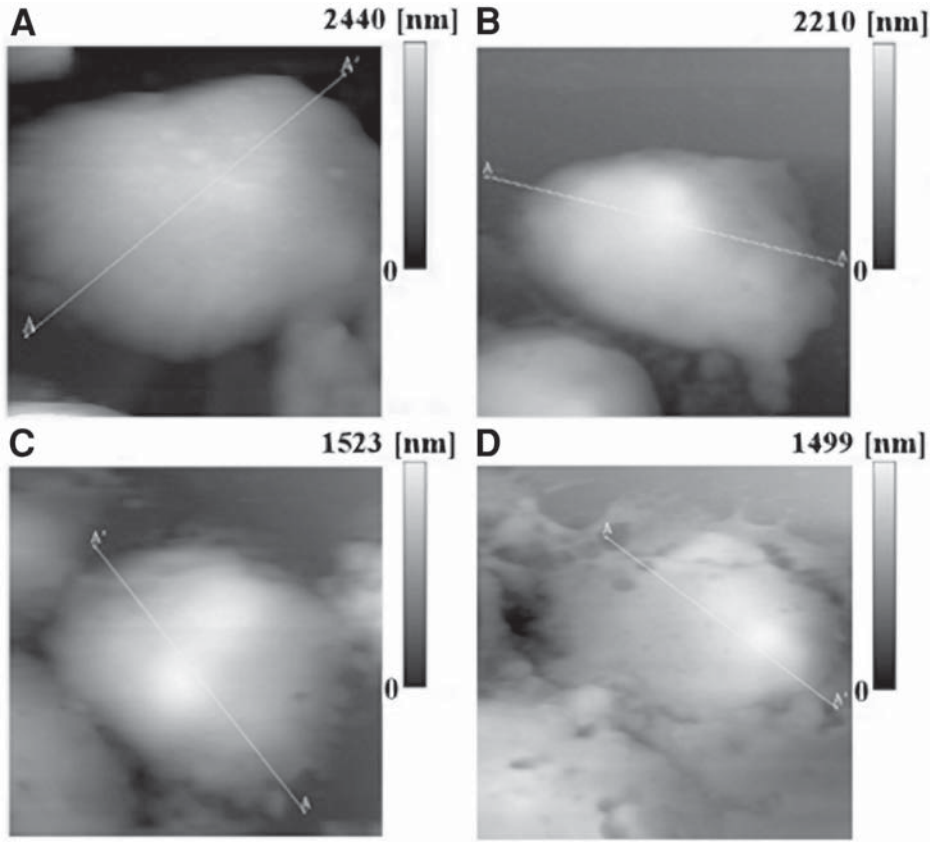

Fig. 1. Constant force AFM images of untreated (**A**, 10 × 10 μm) and, respectively, 9 h (**B**, 13 × 13 μm), 24 h (**C**, 14 × 14 μm), and 64 h (**D**, 13 × 13 μm)-exposed Raji cells. The gray scale is defined so that lighter colors correspond to higher corrugations. It is worth noting that the top height reported for the cells progressively decreases at increasing exposure. In **(A)**, microvilli are visible as a lighter spot on the cell membrane that are no more recognizable after 9–15 h **(B)**. At very long exposure the cell surface become characterized by several "furrows" and infolding **(D)**. A cross-section of these cells, taken along the white line A–A', is shown in **Fig. 4**.

border of the cells, anchoring structures named pseudopodia that are, similarly to microvilli, involved in cell migration.

Cells exposed for 9 h (**Fig. 1B** and **2B**) to MF show clear differences compared to untreated cells: in this case, the microvilli have almost completely disappeared from the surface of the cells and also pseudopodia are hardly detectable.

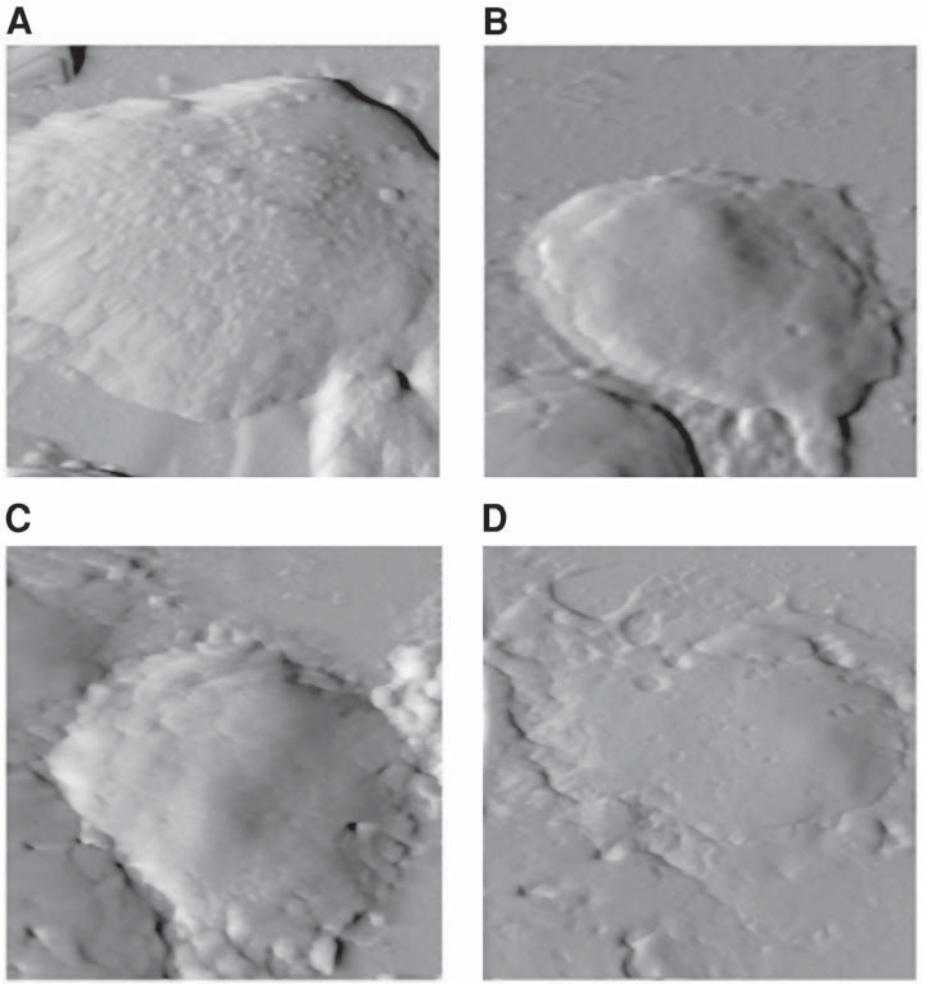

Fig. 2. Lateral friction AFM images of the same cells shown in **Figs. 1A–D**, respectively. Lateral friction images (collected simultaneously to topography) are very sensitive to small structures protruding from a large and corrugated surface so that they are very suitable for describing microvilli **(A)**, as well as the fine surface modifications induced by MF exposure (for instance the pits structure in **D**).

3.2. Cell Membrane Features

The cell membrane, which because of the microvilli could not be directly observed in untreated samples, appears quite smooth with no structures or protrusions on the surface. In cells exposed for 15 h to MF (not shown) both microvilli and pseudopodia can no longer be recognized whereas, as in samples

exposed for a shorter time, the dome shape is essentially unchanged. After 24 h of exposure to MF (**Figs. 1C** and **2C**), a slow membrane change is still going on as revealed by the presence, in some cases, of ripples on the surface (better recognized in the lateral friction image) and by a progressive flattening of the cells. Such a membrane modification is accompanied, in cells exposed for 44 h, by the appearance of "furrows" and pit-like structures (narrow membrane infolding) that become more common in lymphoblasts exposed for 64 h to the field (**Figs. 1D** and **2D**). These features could be considered as markers of the long exposure effect. After 64 h of exposure another important change in cell structure, namely the loss of the spherical shape of the cell, becomes evident. It is worth noting that, in some cases, this change can already be found after 44 h of exposure.

The noticeable modifications of the membrane surface because of MF exposure are shown in the high resolution (3×3 μm) 3D images of **Fig. 3**, in which the surface of an unexposed cell is compared with that of cells exposed for 9, 44, or 64 h. A comparison between **Fig. 3A** and **3B** clarifies the effect of short time exposure, which essentially results in the loss of microvilli.

3.3. Microvilli and Adhesion

An interesting question regards the possibility that the magnetic field exposure changes the proportion of cells adhering to the substrate through the disappearance of microvilli that are involved in cell adhesion and migration: we did not find changes in adhesion although it is not possible to completely exclude such an effect.

3.4. Surface Modification Analysis

The surface modifications after longer exposure are shown in **Figs. 3C** and **3D**, consisting in a slow "aging" of the membrane, which becomes progressively more ruffled and characterized by several narrow introflections easily recognizable in samples exposed for 44 and 64 h.

Figure 4 shows the profiles, taken along the white lines drawn in **Fig. 1**, of the four cells shown in **Figs. 1** and **2**. These data allow at least two important observations about the overall morphological changes of the cells. The first one is the progressive and relevant decrease in the maximum height of the cell with increasing exposure. During the first 9–15 h, such a decrease can be related to the observed loss of microvilli, but the residual changes must reflect modifications of other cellular structures. The second observation regards the cell's domed shape. In fact, unexposed or briefly exposed cells have high dome (**Fig. 4A** and **B**), whereas a loss of the spherical shape starts to be detectable after about 44 h (data not shown) and reaches a maximum after 64 h of exposure. Observing the profile reported in **Fig. 4D**, it is quite evident how this loss

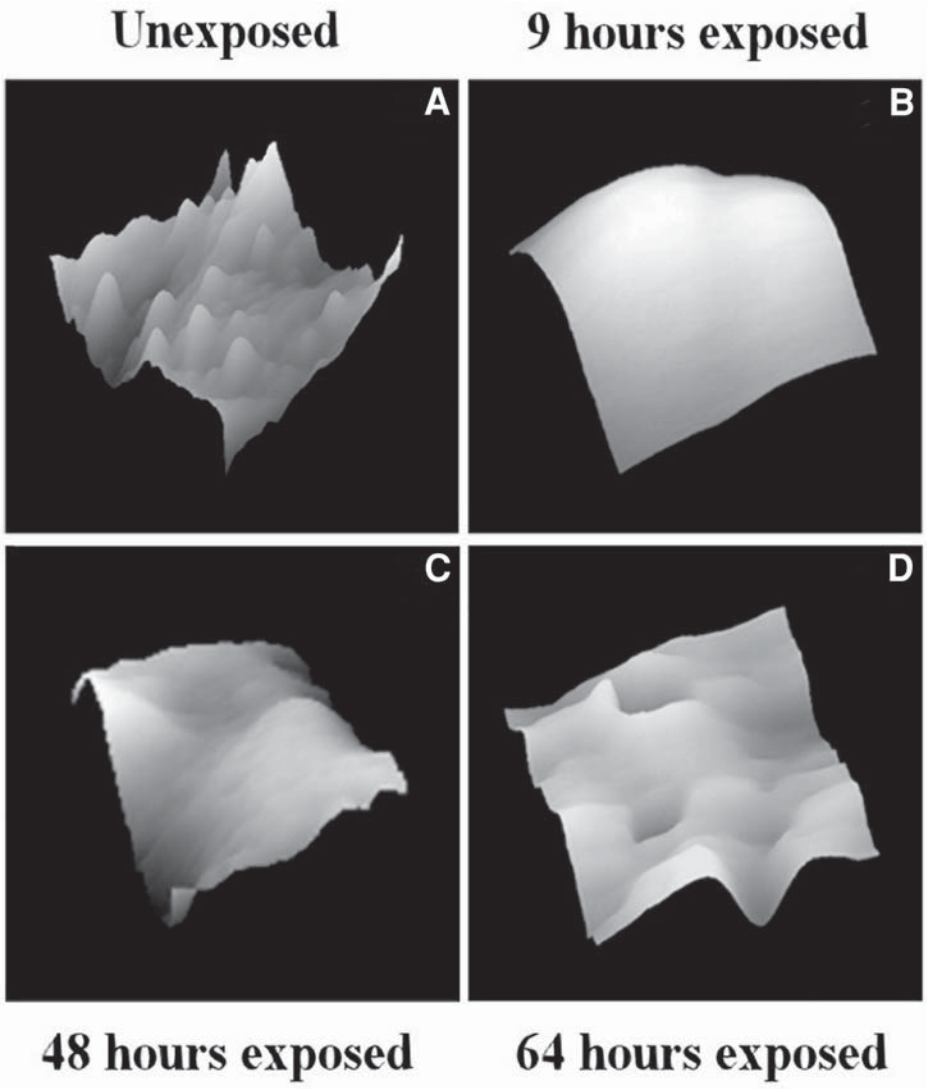

Fig. 3. Constant force images (4 × 4 μm) in a side view 3D representation of the membrane surface of an untreated cell **(A)**, after 9 h **(B)**, 48 h **(C)** and 64 h **(D)** of exposure to MF. The noise in these images is 0.1–0.3 nm. Microvilli are clearly visible in the untreated sample, whereas after 9 h exposure the surface shows flat and smooth. The progressive membrane ageing revealed by surface rippling and the appearance of pit-like structures is evident in images **(C)** and **(D)**.

of spherical shape is the result of a weakening of the support exerted by the cytoskeleton, the cellular structure responsible for the maintenance of the cell shape.

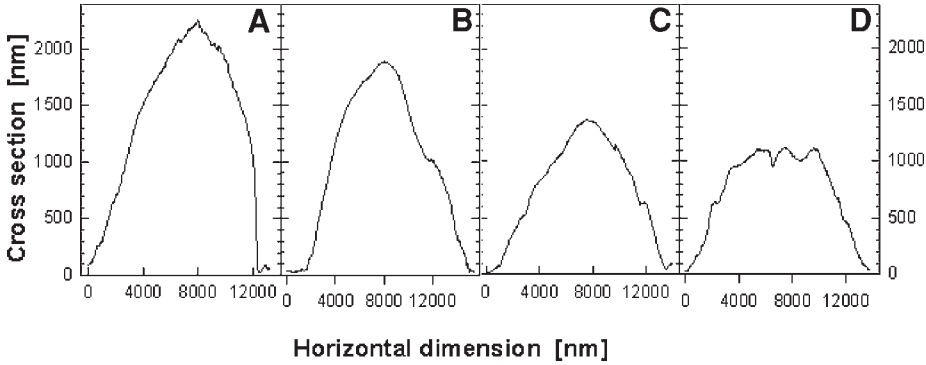

Fig. 4. Cross-sections of the four cells presented in **Fig. 1A–D**, respectively (the profiles are taken along the white line A–A'). This picture clearly shows the main morphological modifications induced by MF. They consist in the (maximum) cell height decreasing at increasing exposure as well as in the loss of cell shape taking place after long time exposure **(D)**. The decrease in height is about complete after 24 h whereas the spherical shape is essentially conserved. At longer exposure, the residual modifications affect only the domed shape of the cell **(D)**. A comparison of the cross-sections of **(C)** and **(D)** shows clearly that the loss of the dome shape arises from loss of support exerted by the cytoskeleton, that is, from a breakdown of this structure.

It seems important to comment the possibility that drying might affect differently the surface structure of control and treated cells: the control cells were treated in exactly the same way as the exposed samples (except, of course, for the exposure). In this way, any difference after drying could only be caused by the exposure. A slightly higher, drying-induced, ruffling of the membrane in cells exposed for 44 or 64 h to MF cannot be excluded because of the changes in the cytoskeleton in those cells. However, we believe that this effect also, if it exists at all, has to be ascribed to the MF-induced modification of the cytoskeleton and not to the drying procedure.

3.5. Artifacts

Another point regards the possibility that while fixing and drying samples many changes might occur in the cell membrane: in the present study, we prepared air-dried samples with a weakly stressing method in order to reduce, as much as possible, any morphological artifact or effect on cell viability. Of course it would be better to study the living cells with the AFM, even though we consider that important information can also be obtained on dried samples. For instance, on dried neurones, there are many aspects that have been studied with ultra-high-vacuum techniques such as spectromicroscopy with synchrotron radiation (*see*, for instance, **refs. *40*** and ***41***).

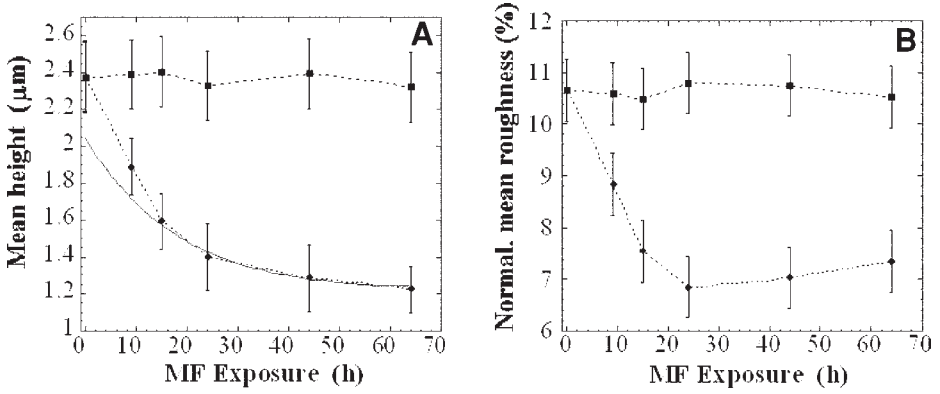

Fig. 5. Normalized roughness **(B)** and mean cell height **(A)** plotted as function of exposure time. Each point is the average of about 50 cells. In both graphs the square symbols represent the control samples and the circles refers to the exposed cells. The controls only show variations within the experimental error. In **(A)**, we report (solid line) the fit executed on the last four data points (the ones free from effects on microvilli). The best fit was obtained with the function $y = m1 + m2 \times e^{-t/18}$ with the following parameters: $m1 = 1.20$; $m2 = 0.84$; $\Delta m1 = 0.06$; $\Delta m2 = 0.03$. The extrapolated value of $H0$ (the zero exposure cells height that does not take into account the microvilli) is 2.04 μm. The results of the fit are discussed in the text.

Concerning cell height and roughness, the results indicate that during the first 24 h both trends are very similar and give rise to a fast and large decrease of the parameters. We suggest that these changes are characterized by two simultaneous effects of MF on microvilli and cytoskeleton respectively. During the following 49 h, the trends become different: in fact decrease in height continues, although very weakly, while the normalized cell roughness undergoes a small increase in agreement with the progressive rippling and appearance of pit structures on the membrane surface.

3.6. Quantitative Evaluation

To allow a more quantitative evaluation of the MF-induced effects, we performed a statistical analysis of the relation between cell modification and exposure time. The results, in terms of mean cell height and normalized roughness (defined as the ratio between the height variance and the mean height value on the portion of surface analyzed), are shown in **Fig. 5A** and **B**. During the first 15–24 h, in which the main part of the MF-induced effect takes place, both graphs show similar decreasing trends. The similarity between the trends in this time frame also implies that the two phenomena of decrease in cell height and loss of structure of the membrane surface occur simultaneously. At longer exposure times, however, the trends of mean height and normalized roughness differ. The height decrease continues, although very weakly, while

the roughness, after reaching a minimum value, shows a small but significant increase. This behavior is not surprising compared with the morphological data of **Fig. 3**, which, in fact, suggest a small increase of the roughness after long exposure in agreement with the progressive membrane rippling and formation of pit structures. This observation demonstrates the sensitivity of our statistical analysis to fine morphological modifications.

In the graph of cell height two different rates of variation are recognizable: a faster one during the first 15 h and a slower one after longer exposure. Because the height decrease continues even after the disappearance of microvilli, an important but time-limited phenomenon, it is clear that the MF acts also on other cellular structure. This structure is the cytoskeleton, subject to a slow but continuous modification. During the first 15 h, the superposition of these two effects causes the faster rate of height variation that is one of the most important results reported.

To avoid the possible interpretation that the data results from a decrease in cell volume, we measured the (apparent) cellular volume individually using an approximation of the cells as spheres or hyperboloids. The results (not shown) reveal volume changes within the experimental error, which means that as height decreases the cells become progressively wider at increasing exposure.

3.7. Role of Calcium

An interpretation of the effects we observed brings into play the role of calcium. Microvilli and pseudopodia are in fact dynamic structures, mainly composed of poly-actin filaments, that can be rapidly created and destroyed ***(46)*** because of Ca^{2+} concentration fluctuations that are known to be induced by exposure to MF ***(3,4,21,22)***. Because actin is present both in the microvilli and in the rest of the cytoskeleton, it is reasonable to believe that the cytoskeleton undergoes the same depolymerization effect observed in the microvilli. However, in the case of the cytoskeleton, the effect is expected to be smaller because of the rigidity of this structure, and it can be unequivocally identified only after long MF exposure (i.e., when the microvilli have already disappeared).

3.8. Estimation of the Effect Induced by MF on the Cytoskeleton

A possible, although rough, estimate of the effect induced by MF on the cytoskeleton during the first 15 h may be attempted by fitting the last four points of the height curve, which are the ones completely free from effects on microvilli. The result of the proposed fit, performed with a simple mono-exponential function (**Fig. 5A** and its caption) show the two rates of the phenomenon. In fact, the best fit obtained, which does not take into account the microvilli, describes very well the range of 13–64 h (for construction) but

clearly indicates a rate of height variation slower than the experimental one in the first hours of exposure. The difference between these two rates of height variation can be ascribed (in large part, at least) to the effect on microvilli.

The use of the fit also allows extrapolation of a zero exposure height value (H0) that takes into account only the effect on the cytoskeleton. The total height variation during the first 9–15 h of exposure can be written as follows:

$$\Delta H_{tot} = \Delta H_c + \Delta H_m \quad (1)$$

where ΔH_{tot} is the total height variation; ΔH_c is the contribution to the height variation because of the cytoskeleton and ΔH_m is the contribution to the height variation attributable to the microvilli.

At $t = 0$ ΔH_c can be estimated by the zero exposure fit extrapolation $H0$ (equal to 2.04 μm) and the contribution because of the microvilli ($\Delta H_m = \Delta H_{total} - \Delta H_c$) results to be about 0.34 μm (with an error of 0.09), a value close to the 0.4 μm suggested by Knutton et al. ***(47)***. It is worth noting that this value should be considered as an independent estimation of the size of microvilli in the sample analyzed.

3.9. Comparison With SEM and Fluorescence Microscopy

It is worth noting that our results are in agreement with previous data of Santoro et al. ***(10)*** that report, by scanning electron microscopy of lymphoblastoid cells, the loss of microvilli after 72 h exposure to 50 Hz, 2 mT MF and also show, by fluorescence microscopy analysis, a rearrangement of actin subsequent to (72 h) exposure. This supports the interpretation of our data with regard to effects on the cytoskeleton. In the same paper the authors also provide Laurdan spectroscopy evidence of a membrane fluidity variation that can be related to the progressive modification of the membrane leading to the appearance of rippling and pit-like structures reported here.

In this view, our data enable us to extend, and roughly quantify, the detection of cytoskeletal modifications during the first hours of exposure and to add a 3D description of the MF-induced changes. We can also introduce an experimental correlation between exposure time and morphological parameters such as cell height, shape, membrane roughness, and carry out the variation kinetics of these parameters to determine markers of long MF exposure.

4. Comments

The AFM images reported here demonstrate the existence of an exposure-dependent MF-induced morphological effect on immune system cells (Raji). This effect can roughly be divided as follows: within the first 10–15 h there is a large decrease of cell height and roughness related to the disappearance of microvilli with a minor simultaneous effect on the cytoskeleton. At longer

exposure time the plasma membrane appears to become completely free of microvilli and the weak residual variation, which can be completely ascribed to the cytoskeleton, leads to a less domed and wider cell shape and to the appearance of ripples and pit structures on the membrane surface.

The reported data allow us to speculate that in such treated cells some functional alteration occurs (for instance in cell motility or target recognition). However, the very large diffusion in intensity and frequency of the MF used in our study requires caution in drawing conclusions about a possible health hazard.

Further information about actual cell damage induced by MF will come from the characterization of the degree and the kinetics of reversibility of the morphological changes, and also from the study of the correlation of morphological changes to biochemical modifications and cellular dysfunction. It could also be interesting to establish the threshold value of the field intensity below which no morphological modification is detectable. Specific studies are in progress to extend the experiment to different cell lines that, because of the known specificity of the MF-induced effect, could present a different response pathway.

Acknowledgment

This work has been partially supported by a grant from Istituto Superiore Prevenzione E Sicurezza del Lavoro (ISPESL).

References

1. Bassett, C. A. L., Mitchell, S. N., and Gaston, S. R. (1982) Pulsing electromagnetic field treatment in ununited fractures and failed arthrodeses. *JAMA* **247,** 623–628.
2. Liboff, A. R. (1985) Cyclotron resonance in membrane transport, in *Interaction Between Electromagnetic Fields and Cells* (Chiabrera, A., Nicolini, C., and Schwan, H. P., eds.) NATO ASI, series A 97, Plenum Press, New York, pp 281.
3. Walleczeck, J. (1992) Electromagnetic field effect on cells of the immune system: the role of calcium signaling. *FASEB J.* **6,** 3177–3185.
4. Glaser, R. (1992) Current concepts of the interaction of weak electromagnetic fields with cells. *Bioelectrochem. Bioenerg.* **27,** 255–268.
5. Paradisi, S., Donelli, G., Santini, M. T., Straface, E., and Marloni, W. A. (1993) A 50 Hz magnetic field induces structural and biophysical changes in membranes. *Bioelectromagnetics* **14,** 247–255.
6. Tenforde, T. S. (1995) Interaction of extremely low frequency electric and magnetic fields with humans, in *Handbook of Biological Effects of Electromagnetic Field*, 2nd ed, Chapter 4 (Polk, C. and Postow, E., eds.) CRC Press, Boca Raton, FL, pp. 185–230.
7. Polk, C. (1995) Electric and magnetic fields for bone and soft tissue repairs, in *Handbook of Biological Effects of Electromagnetic Field*, 2nd ed., Chapter 5 (Polk, C. and Poston, E., eds.) CRC Press, Boca Raton, FL, pp. 231–246.

8. Stevens, R. G. (1995) Epidemiological studies of electromagnetic fields and health, in *Handbook of Biological Effects of Electromagnetic Field*, 2nd ed., Chapter 7 (Polk, C. and Poston, E., eds.) CRC Press, Boca Raton, FL, pp. 275–294
9. Kaiser, F. (1996) External signals and internal oscillation dynamics: Biophysical aspects and modelling approaches for interactions of weak electromagnetic fields at the cellular level. *Bioelectrochem. Bioenerg.* **41,** 3–18.
10. Santoro, N., Lisi, A., Pozzi, D., Pasquali, E., Serafino, A., and Grimaldi S (1997) Effect of extremely low frequency magnetic field exposure on morphological and biophysical properties of human lymphoid cell line (Raji). *Biochem. Biophys. Acta* **1357,** 281–290.
11. Tofani, S. and D'Amore, G. (1991) Extremely low frequency and very low frequency magnetic fields emitted by video display units. *Bioelectromagnetics* **12,** 35–45.
12. Vistnes, A. I., Ramberg, G. B., Bjornevik, L. R., Tynes, T., and Haldorsen T. (1997) Exposure of children to residual magnetic fields in Norway: Is proximity to power lines an adequate predictor of exposure? *Bioelectromagnetics* **18,** 47–57.
13. Savitz, D. A., John, E. M., and Kleckner, R. C. (1990) Magnetic field exposure appliances and childhood cancer. *Am. J. Epidemiol.* **191,** 763–773.
14. Coghill, R. W. (1996) Low frequency electric and magnetic fields in the bedplace of children with leukaemia. *Biophysics.* **41,** 809–816.
15. Kavet, R. (1996) EMF and current cancer concept. *Bioelectromagnetics* **17,** 339–357
16. Rosenthal, M. and Obe, G. (1989) Effects of 50-Hertz electromagnetic fields on proliferation and chromosomal alterations in human peripheral lymphocytes untreated or pretreated with chemical mutagens. *Mutat. Res.* **210,** 329–335.
17. Loscher, W. and Mevissen, M. (1995) Linear relationship between flux density and tumor co-promoting effect of prolonged magnetic field exposure in a breast cancer model. *Cancer Lett.* **96,** 175–179
18. Blank, M. (1987) The surface compartment model: a theory of ion transport focused on ionic processes in the electric double layers at membrane protein surface. *Biochem. Biophys. Acta* **906,** 277–294
19. Lednev, V. V. (1996) Bioeffects of weak combined, constant and variable magnetic fields. *Biophysics* **41,** 241–252.
20. Barnes, F. S. (1996) Effect of electromagnetic fields on the rate of chemical reactions. *Biophysics* **41,** 801–808.
21. Carson, J. J. L., Prato, F. S., Drost, D. J., Diesbourg, L. D., and Dixon, S. J. (1990) Time varying magnetic fields increase cytosolic free Ca^{2+} in HL-60 cells. *Am. J. Physiol.* **259,** 687–692.
22. Cadossi, R., Bersani, F., Cossarizza, A., et al. (1992) Lymphocytes and low frequency electromagnetic fields. *FASEB J.* **6,** 2667–2674.
23. Alipov, Y. D. and Belyaev, I. Y. (1996) Difference in frequency spectrum of extremely low frequency effects on the genome conformational state of AB1157 and *E. coli* cells. *Bioelectromagnetism* **17,** 384–387.

24. Shao, Z., Mou, J., Czajkowsky, D. M., Yang, J., and Yuan, J. Y. (1996) Biological atomic force microscopy: What is achieved and what is needed. *Adv. Phys.* **45,** 1–86.
25. Butt, H. J., Wolff, E. K., Gould, S. A. C., Dixon Nothern, B., Peterson, C. M., and Hansma, P. K. (1990) Imaging cells with the atomic force microscope. *J. Struct. Biol.* **105,** 54–61.
26. Gould, S. A. C., Drake, B., Prater, C. B., et al. (1990) From atoms to integrated chips, blood cells and bacteria with the atomic force microscope. *J. Vac. Sci. Tecnol. A.* **8,** 369–373.
27. Bustamante, C., Vesenka, J., Tang, C. L., Rees, W., Guthold, M., and Keller, R. (1992) Circular DNA molecules imaged in air by scanning force microscopy. *Biochemistry* **31,** 22–28.
28. Henderson, E., Haydon, P. G., and Sakaguchi, D. S. (1992) Actin filament dynamics in living glial cells imaged by atomic force microscopy. *Science* **257,** 1944–1946.
29. Cricenti, A., De Stasio, G., Generosi, R., Perfetti, P., Ciotti, M. T., and Mercanti D (1995) Atomic force microscopy of neuron networks. *Scanning Microsc.* **9,** 695–700.
30. Zecca, L., Dal Conte, G., Furia, G., and Ferrario, P (1985) The effect of alternating magnetic field on experimental inflammation in the rat. *Bioelectrochem. Bioenerg.* **14,** 39–43.
31. Stuchly, M. A., Ruddick, J., Villeneuve, D., et al. (1988) Teratological assessment of exposure to time-varying magnetic field. *Teratology* **38,** 461–466.
32. McLean, J. R. N., Stuchly, M. A., Mitchel, R. E. J., et al. (1991) Cancer promotion in a mouse skin model by 60-Hz magnetic field: II. Tumor development and immune response. *Bioelectromagnetics* **12,** 273–287.
33. Santini, M. T., Cannetti, C., Paradisi, S., et al. (1995) A 50 Hz sinusoidal magnetic field induces changes in the membrane electrical properties of K562 leukaemic cells. *Bioelectrochem. Bioenerg.* **36,** 39–45.
34. Weiss, A. and Imboden, J. B. (1987) Cell surface molecules and early events involved in human T lymphocyte activation. *Adv. Immunol.* **41,** 1–38.
35. Greene, J. J., Skowronski, W. J., Mullins, J. M., Nardone, R. M., Penafiel, M., and Meister, R. (1991) Delineation of electric and magnetic field effects of extremely low frequency electromagnetic radiation on transcription. *Biochem. Biophys. Res. Commun.* **174,** 742–749.
36. Conti, P., Gigante, G. E., Alesse, E., Cifone, M. G., Fieschi, C., Reale, M., and Angeletti, P. U. (1985) A role for calcium in the effect of very low frequency electromagnetic field on the blastogenesis of human lymphocytes. *FEBS Lett.* **181,** 28–32.
37. Lin, P. S., Wallach, D. F. H., and Tsai, S. (1973) Temperature induced variations in the surface topology of cultured lymphocytes are revealed by scanning electron microscopy. *Proc. Nat. Acad. Sci. USA* **70,** 2492–2496.
38. Weaver, J. C. and Astumian D (1990) The response of living cells to very weak electric fields: The thermal noise limit. *Science* **247,** 459–462.

39. Pulvertaft, R. J. V. (1964) Cytology of Burkitt's tumour (African lymphoma). *Lancet* **1,** 238–240.
40. Mercanti, D., De Stasio, G., Ciotti, M. T., et al. (1991) Photoelectron microscopy in the life science: Imaging neuron network. *J. Vac. Sci. Technol. A* **9,** 1320–1322
41. Lo Russo, G. F., De Stasio, G., Casalbore, P., et al. (1997) Photoemission analysis of chemical differences between the membrane and cytoplasm of neuronal cells. *J. Phys. D* **30,** 1794–1798
42. Cricenti, A. and Generosi R (1995) Air operating atomic force-scanning tunneling microscope suitable to study semiconductors, metals and biological samples. *Rev. Sci. Instrum.* **66,** 2843–2847.
43. Cricenti, A., De Stasio, G., Generosi, R., et al. (1996) Native and modified uncoated neurons observed by atomic force microscopy. *J. Vac. Sci. Technol. A.* **14,** 1741–1746.
44. De Stasio, G., Cricenti, A., Generosi, R., et al. (1995) Neurone decapping characterization by atomic force microscopy: A topological systematic analysis. *NeuroReport.* **7,** 65–68.
45. Bretscher, M. S. (1996) Getting membrane flow and the cytoskeleton to cooperate in moving cells. *Cell* **87,** 601–606.
46. Allen, L. A. and Aderem A (1995) A role for MARCKS, the {a} isozyme of protein kinase C and myosin I in zymosan phagocytosis by macrophages. *J. Exp. Med.* **182,** 829–840.
47. Knutton, S., Summer, M. C. B., and Pasternak, C. A. (1975) Role of microvilli in surface changes of synchronized P815Y mastocytoma cells. *J. Cell Biol.* **66,** 568–576.